

# The Rotating Vicsek Model: Pattern Formation and Enhanced Flocking in Chiral Active Matter

Benno Liebchen<sup>1,\*</sup> and Demian Levis<sup>2,†</sup>

<sup>1</sup>*SUPA, School of Physics and Astronomy, University of Edinburgh, Edinburgh EH9 3FD, United Kingdom*

<sup>2</sup>*Departament de Física de la Matèria Condensada,  
Universitat de Barcelona, Martí i Franquès 1, E08028 Barcelona, Spain*

(Dated: March 2, 2023)

We generalize the Vicsek model to describe the collective behaviour of polar circle swimmers with local alignment interactions. While the phase transition leading to collective motion in 2D (flocking) occurs at the same interaction to noise ratio as for linear swimmers, as we show, circular motion enhances the polarization in the ordered phase (enhanced flocking) and induces secondary instabilities leading to structure formation. Slow rotations result in phase separation whereas fast rotations generate patterns which consist of phase synchronized microflocks of controllable self-limited size. Our results defy the viewpoint that monofrequent rotations form a rather trivial extension of the Vicsek model and establish a generic route to pattern formation in chiral active matter with possible applications to control coarsening and to design rotating microflocks.

Among the most remarkable features of active matter systems is their ability to spontaneously form self-sustained non-equilibrium structures, without requiring any external driving. These structures range from motility induced phase separation [1, 2] and clusters with self-limited length scales [3–7] in isotropic active matter, to long range ordered flocks and traveling bands in two dimensions for polar self-propelled particles, as described by the Vicsek model [8–12]. The Vicsek model in particular, has become the archetypical (polar) active matter model: much of our understanding of collective behaviour and universality in active system comes from its extensive investigation.

Besides ‘linear’ self-propelled particles which reorient their swim direction only by diffusion, there is now much interest in swimmers which change their direction of motion autonomously. This has led to the new subfield of chiral active matter including a plethora of biological swimmers. *E.coli*, for example, naturally swim in circles when close to walls and interfaces [13–16], and sperm cells generically describe circular and helical trajectories in two and three dimensions [17, 18]. Generally, such circular trajectories emerge as a consequence of any small deviation between the self-propulsion direction of a swimmer and its symmetry axis, thus coupling translational and rotational degrees of freedom. Based on this general principle, it has been possible to create synthetic circle swimmers, including L-shaped self-phoretic swimmers [19] and actuated colloids allowing to design radius and frequency of circular trajectories on demand. Despite a recent boost in research on circle swimmers [20, 21], surprisingly little is known about their collective behaviour (a notable exception exploring collective behaviour is [22]).

Therefore, we introduce here a generalized Vicsek

model for circle swimmers, which we call the *rotating Vicsek model*. As self-propelled circle swimmers are automatically nonspherical, particles locally align with their neighbors in our model. They also chance their direction of motion autonomously with an intrinsic rotation frequency, accounting for circular swimming. In the monofrequent case of identical swimmers, one might expect that the physics of the Vicsek model remains unchanged, as the absence of inertia seems to guarantee invariance of the system by global rotation of the reference frame - this is similar as for overdamped passive particles in a rotating bucket. Such a viewpoint is further supported by our finding that identical circle swimmers feature the same flocking transition as the Vicsek model, independently of their frequency. Once polar order has emerged, however, circular swimming dramatically influences the collective behaviour of polar active matter (even in the case of identical rotations): In particular, when rotations are fast compared to rotational diffusion, which is a natural parameter range for many circle swimmers, a new phase emerges, which we call the *rotating micro-flock* phase. This phase emerges via a short-wavelength clustering instability from a uniform flock and leads to a proper pattern of localized rotating flocks which do not coarsen beyond a characteristic length scale (which scales linearly with the swimming speed and decreases often sublinearly with the rotational frequency). Besides this new phase occurring in the large frequency domain, also slow rotations induce interesting collective effects: they allow for coherently moving large-scale structures with droplet-like shapes featuring enhanced polarization as compared to the standard Vicsek model. If rotations are fast enough, these structures can even survive at interaction to noise ratios where the standard Vicsek model is deeply in the uniform flocking regime. Thus, in contrast to the common opinion that identical circular swimming does not change the collective behaviour of linear swimmers significantly, we show that they lead to a rich new phase diagram, involving

\*Benno.Liebchen@staffmail.ed.ac.uk

†levis@ub.edu

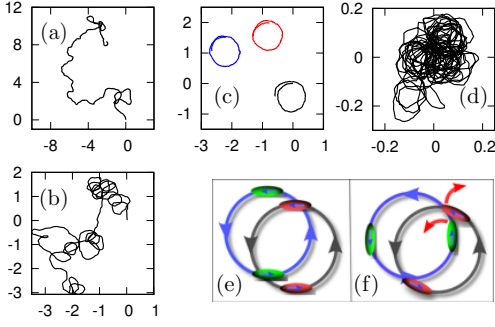


FIG. 1: Trajectories of a single linear Brownian swimmer (a,  $\Omega = 0$ ) and a single circle swimmer (b,  $\Omega = 3$ ). (c): For slow rotations ( $g = 0.14$ ,  $\Omega = 0.2$ ), circle swimmers phase synchronize and swim on almost ideal circles, leading to a drop-like flock where particles swim in parallel, satisfying the alignment interactions (e). (d): For fast rotations ( $g = 0.14$ ,  $\Omega = 3$ ), circle swimmers have no time to phase lock. The resulting phase shift frustrates the alignment interactions and make circular trajectories impossible (f). The global flock breaks down and circle swimmers form microflocks, where they are, on average, aligned with their neighbors and circle irregularly around the center of the microflock.

a novel route to pattern formation. This route should be readily observable in identical synthetic circle swimmers (L-shaped or actuated colloids) or in magnetotactic bacteria in rotating external magnetic fields [23, 24], and could be useful, for example, to design localized microflocks whose characteristic size can be (dynamically) controlled in the laboratory (by changing the self-propulsion velocity or the frequency of the rotating field). (Note that our results might even apply to nonidentical synchronized swimmer ensembles as discussed in [32].) Besides this, our results might be useful for understanding pattern formation in 2D suspensions of sperm cells [18] and driven protein filaments [22, 25] which qualitatively match the microflocks we observe.

*The rotating Vicsek model* To specify our results we now introduce the rotating Vicsek model. We consider  $N$  point-like self-propelled particles with positions  $\mathbf{r}_i$  and orientations  $\mathbf{p}_i(t) = (\cos \theta_i, \sin \theta_i)$  which interact via an aligning pair-potential and change their direction in response to a systematic rotational force and rotational noise, according to:

$$\dot{\mathbf{r}}_i = v\mathbf{p}_i, \dot{\theta}_i = \omega + \frac{K}{\pi R_\theta^2} \sum_{j \in \partial_i} \sin(\theta_j - \theta_i) + \sqrt{2D_r}\eta_i, \quad (1)$$

Here, the sum runs over neighbors within a radius  $R_\theta$  around particle  $i$  and  $\eta_i$  is a unit-variance Gaussian white noise with zero mean. In the non-interacting limit, each particle performs an overdamped circular Brownian motion as shown in Fig. 1 and statistically characterised in [34]. To reduce the parameter space to its essential dimensions, we choose space and time units as  $R_\theta$  and  $1/D_r$ . Besides the particle density  $\rho_0 = N/L^2$ , we have three control parameters: a Peclet number  $\text{Pe}_r =$

$v/(D_r R_\theta)$  measuring the persistence length in units of the alignment interaction range,  $g = K/(\pi R_\theta^2 D_r)$  and  $\Omega = \omega/D_r$ , comparing alignment and rotational frequencies with the rotational diffusion rate. We show below that phase boundaries in the rotating Vicsek model depend only on two effective parameters,  $g\rho_0$  and  $\Omega$ . Most interesting phenomena occur for  $g\rho_0 > 2$  (which is the same requirement as to observe flocking in the standard Vicsek model) and for  $\Omega \sim 1$  or  $\Omega > 1$ . Rotating *E.coli* with  $\omega \sim 0.1 - 1/s$  [15] and  $D_r \sim 0.2/s - 1/s$  lead to  $\Omega \sim 1$ , L-shaped swimmers with  $\omega \sim 0.1 - 0.3/s$  and  $D_r \sim 6 \cdot 10^{-4}$  [19] allow to explore the regime  $\Omega \sim 10^2 \gg 1$  (less asymmetric colloids would allow to explore the regime  $\Omega \sim 1$  as well) and magnetotactic bacteria in rotating fields should be well suited to explore the whole range of  $\Omega$ .

*Pattern formation* We now explore the impact of identical rotations on the standard Vicsek model by simulating ensembles of  $N = 32000$  circle swimmers in a quadratic box with periodic boundary conditions. For  $\Omega = 0$  we reproduce the phenomenology of the standard Vicsek model [12, 33, 35, 36]: a disordered homogeneous phase occurs below the flocking threshold ( $g < g_f$ ), whereas  $g \gtrsim g_f$  induces a global polarization with high density bands coexisting with a disordered gas (Fig. 2 (a)). These density patterns in the form of traveling bands eventually become unstable at higher coupling strengths, leading to homogenous flocking. Now choosing  $g > g_f$  and switching on slow rotations ( $\Omega = 0.2$ ), the system phase separates into a large polarly ordered dense phase and a low-density gas of incoherently rotating particles. Here, the presence of rotations changes the geometry of the high density region which now takes the form of a spherical cluster, reminiscent of the usual liquid-gas demixing, that rotates coherently with a frequency  $\Omega^* < \Omega$  (see Fig. 1 (c), 2 (b) and Movie 1 in the Supplementary Material (SM) [39]). Strikingly, for  $\Omega > 1$ , particles self-assemble into localized dense structures and form a pattern of spots, which do not grow beyond a characteristic size (see Fig. 2 (c)-(h) and Movie 2). These patterns are reminiscent of vortex arrays observed in sperm cells and protein filaments [18, 25]. One can associate a characteristic length scale to such structures that we quantify it by  $\lambda$ , defined as  $G(\lambda) = 1$ , where  $G$  is the pair correlation function. As shown in Fig. 2 (c)-(e) and (i), faster particles collect their neighbours into larger microflocks, as the radius of their trajectories increases. Similarly,  $\lambda$  decreases with the rotation frequency and grows with the coupling strength (see Fig. 2 (f)-(h) and (j)). Thus, the typical size of the microflocks can be simply controlled by the microscopic parameters of the model [40].

*Hydrodynamic equations and enhanced flocking* To understand the emergence of patterns and the underlying instability mechanisms, we systematically derive a continuum theory for our rotors in the SM [39]. Following the approaches in [29, 31] we find a closed set of equations for the density  $\rho(\mathbf{x}, t)$  and polarization density

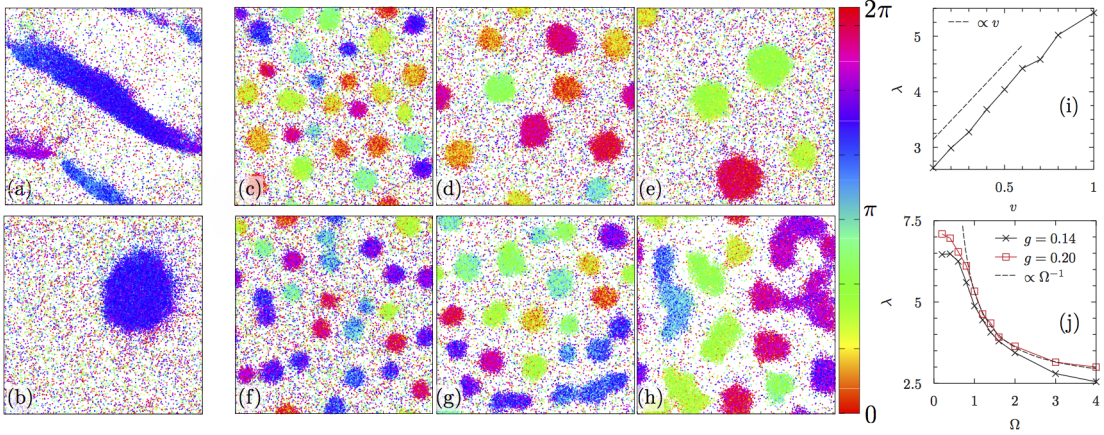


FIG. 2: Representative snapshots of a system of  $N = 32000$  particles at fixed  $\rho = 20$  and  $D_r = 0.5$ . Particles are represented by a colored point encoding its orientation. For  $g > g_f$ ,  $\Omega < 1$ , the system phase separates and bands (a,  $\Omega = 0$ ) or droplets (b,  $\Omega = 0.2 < 1$ ) emerge. For both snapshots (a) and (b)  $g = 0.14$ . For  $\Omega > 1$  we observe micro-flocks of controllable size increasing with self-propulsion velocity and alignment interactions. (c-e): Microflocks at  $g = 0.14$ ,  $\Omega = 3$  and  $v = 0.1$  (c),  $v = 0.5$  (d) and  $v = 1$  (e). (f-h): Microflocks at  $v = 0.1$ ,  $\Omega = 3$  and  $g = 0.12$  (f),  $0.18$  (g) and  $0.3$  (h). (i,j): Microflock length scale  $\lambda$  for fixed  $\Omega = 3$  and  $g = 0.14$  as a function of  $v$  (i) and for fixed  $v = 0.1$  and two different coupling strengths as a function of  $\Omega$  (j).

$\mathbf{w}(\mathbf{x}, t) = (w_x, w_y) = \rho \mathbf{P}$  (with  $\mathbf{P}(\mathbf{x}, t)$  being the polarization field) which describe the many particle dynamics in the disordered uniform phase and for moderate deviations from isotropy. The direction of  $\mathbf{w}$  describes the local average of the swimming direction, whereas  $|\mathbf{w}|$  measures the local degree of alignment (polarization times particle density):

$$\dot{\rho} = -\text{Pe}_r \nabla \cdot \mathbf{w} \quad (2)$$

$$\begin{aligned} \dot{\mathbf{w}} = & (g\rho - 2) \frac{\mathbf{w}}{2} - \frac{\text{Pe}_r}{2} \nabla \rho + \frac{\text{Pe}_r}{2b} \nabla^2 \mathbf{w} - \frac{g^2}{b} |\mathbf{w}|^2 \mathbf{w} \quad (3) \\ & + \frac{g\text{Pe}_r}{4b} [5\nabla \mathbf{w}^2 - 10\mathbf{w}(\nabla \cdot \mathbf{w}) - 6(\mathbf{w} \cdot \nabla) \mathbf{w}] \\ & + \Omega \mathbf{w}_\perp + \frac{\text{Pe}_r^2 \Omega}{4b} \nabla^2 \mathbf{w}_\perp - \frac{g^2 \Omega}{2b} |\mathbf{w}|^2 \mathbf{w}_\perp \\ & + \frac{g\text{Pe}_r \Omega}{8b} [3\nabla_\perp \mathbf{w}^2 - 6\mathbf{w}(\nabla_\perp \cdot \mathbf{w}) - 10(\mathbf{w} \cdot \nabla_\perp) \mathbf{w}] \end{aligned}$$

Here  $b = 2(4 + \Omega^2)$ ,  $\mathbf{w}_\perp^{(1)} = (-w_y^{(1)}, w_x^{(1)})$  and  $\nabla_\perp = (-\partial_y, \partial_x)$ . We first notice that the disordered uniform phase (D)  $(\rho, \mathbf{w}) = (\rho_0, \mathbf{0})$  solves eq. (3). Here,  $\rho_0$  is fixed by the initial conditions and conserved in the course of the dynamics. Linearizing eq. (3) around D (SM [39]) leads to exactly the same instability criterion as for straight swimmers ( $\Omega = 0$ ):  $g\rho_0 > 2$ . Our simulations confirm that the flocking transition is independent of rotations as shown in Fig. 3 [41]. When D get unstable, a second spatially uniform solution  $(\rho, |\mathbf{w}|) = (\rho_0, w_0)$  of eq. (3) becomes relevant. This solution represents a flocking phase (F) which features long-range polar order with a polarization density

$$w_0 = \frac{1}{g} \sqrt{(g\rho_0 - 2)(4 + \Omega^2)} \quad (4)$$

and rotates with a frequency  $\Omega_0 = \Omega \left( \frac{3}{2} - \frac{g\rho_0}{4} \right)$ . Thus, the uniform flock rotates with the single particle frequency at the onset of flocking but slows down for  $g\rho_0 > 2$ . Strikingly and conversely to the location of the flocking transition, the flocking phase itself is significantly affected by rotations. Eq. (4) suggests an enhanced polarization as  $\Omega$  increases, which we confirm with our simulations in Fig. 3. [42] Physically, this enhanced flocking is based on a decrease of the average time needed for a diffusive rotating particle (which is not yet part of the flock) to align its direction with the flock. That is, rotations allow the flock to collect particles with random orientations faster.

To understand when uniform flocking is observable, we now perform a linear stability analysis of F. Here, in contrast to the linearization around D, first order gradient terms in eq. (3) with coefficients involving  $\Omega$  have linear components. Hence, they have an important influence on small fluctuations around F. In particular, we find an oscillatory long wavelength instability along polarization direction for  $2 < g\rho_0 < 22/7$  for  $\Omega = 0$  which provokes moving density fluctuations and is often associated with the emergence of bands in the Vicsek model, consistently with other continuum approaches [31, 33]. This instability survives only for small  $\Omega$  and is often accompanied by a long-wavelength instability perpendicular to the polarization direction (which has not been discussed much in the literature, despite its existence even at  $\Omega = 0$ ). This transversal instability is oscillatory for circle swimmers but not for straight swimmers, and is responsible for the transition from bands ( $\Omega = 0$ , Fig. 2) to rotating and phase separated drop-structures. These drop-structures feature internal phase synchronization and exist even for small  $\Omega > 0$  as our simulations reveal (Fig. 2 (b)).

Most strikingly, for larger  $\Omega$  these long wavelength in-

stabilities vanish. Instead, our linear stability analysis unveils a rotation-induced oscillatory short wavelength instability perpendicular to the flocking direction which generically destabilizes F and induces a pattern of microflocks with a characteristic size (see Fig. (2)). This finding is quite remarkable, as it shows that the rotating Vicsek model, in contrast to the standard Vicsek model, not only provides a proper route to pattern formation but also allows for structure formation beyond the moderate density regime around the flocking transition. Our analysis generally predict that the characteristic size of the microflocks scales as  $l^* \propto \text{Pe}_r$  and therefore grows linearly with the self-propulsion velocity. Our simulations confirm this scaling as shown in Fig. 2 (i). More generally, we show in the SM that close to  $g\rho_0 = 2$  the size of the microflocks scales as

$$l^* \propto \frac{\text{Pe}_r[\Omega^2(7 - g\rho_0) - 4(g\rho_0 - 2)]}{4\Omega^2\sqrt{(4 + \Omega^2)(g\rho_0 - 2)}}. \quad (5)$$

Meaning that, the characteristic length scale typically grows with  $g\rho_0$  and decreases with  $\Omega$ . For  $\Omega \gg 1$ , the characteristic size of the microflocks is linear in the single swimmer radius, i.e.  $l^* \propto \text{Pe}_r/\Omega \propto v/\omega$ . We confirm both predictions numerically in Fig. 2 (f-h) and (g). Deep in the rotation dominated regime, the microflock size is proportional to the single swimmer radius, which supports the picture, that all particles in the microflock still swim in circles on average.

What is the physical mechanism leading to the rotating droplet phase and the microflock pattern? While circle swimmers are effectively independent of each other at large distances in the uniform phase ( $g\rho_0 < 2$ ), at  $g\rho_0 > 2$  they have to satisfy both alignment interactions and rotations. If interactions are dominant ( $g\rho_0/\Omega \gg 1$ ) circle swimmers phase lock and move on almost perfect circles (Fig. 1 (c)). In this state, they are always parallel to each other (Fig. 1 (e)) and form a macroscopic rotating flock, given by the droplet phase (Fig. 2(b)). (Here, interactions support circular motion: phase locking leads to an essentially stiffly rotating many-particle object, experiencing an 'average' noise which leads to only weak deviations from circular motion.) Conversely, when rotations dominate ( $g\rho_0/\Omega \ll 1$ ) the timescale to achieve phase locking is no longer small compared to the rotational timescale. This results in a phase shift among adjacent circle swimmers, which conflicts with the alignment interactions, for swimmers on circular trajectories, and hence leads to deviations from circular swimming (Fig. 1 (e)). Thus, for fast rotations, we are facing an intrinsic conflict between circular swimming and long range polar order, which leads to the microflock phase. The microflock phase satisfies alignment interactions and circular swimming on average: different swimmers rotate irregularly around a common center while exhibiting polar order (see Fig. 1 (d) for a typical trajectory). Notably, in contrast to weak rotations which support alignment in the droplet phase, fast rotations frustrate alignment. Clearly, the microflocks naturally resist coarsening, as

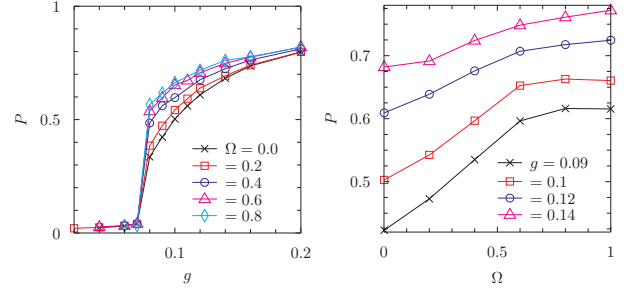


FIG. 3: Flocking transition and enhanced flocking: Global polarization as a function of  $g$  for several frequencies (left) and as a function of  $\Omega$  for several coupling strengths (right). While the transition point is independent of  $\Omega$ , as predicted, rotations enhance global ordering as predicted by Eq. (4). The theory predicts a transition at  $g_f = 2/\rho_0 = 0.1$ , slightly above the numerical result.

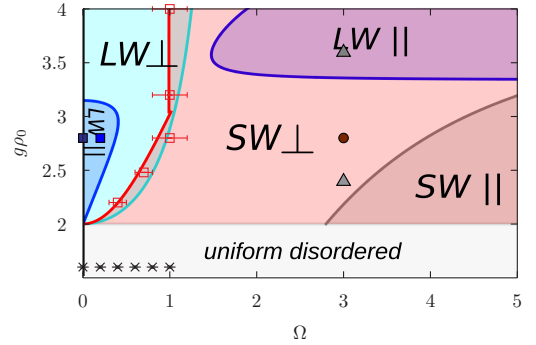


FIG. 4: Nonequilibrium phase diagram as predicted analytically (shaded regions and lines) and by simulations (symbols). Black symbols correspond to the flocking threshold, while red symbols separate states with a single dense cluster from microflock states. Filled symbols indicate the location of the states shown in Fig. 2. Blue symbols: Fig. 2 (a) and (b); brown symbol: Fig. 2 (c-e); grey symbols: Fig. 2 (f-g) (the snapshot Fig. 2 (h) is outside the chosen range). The disordered uniform phase (light gray region) is stable for  $g\rho_0 < 2$  independently of rotations. Long-range polar order emerges for  $g\rho_0 > 2$  (flocking transition): Rotations induce a short wavelength instability perpendicular to the polarization direction (red,  $\text{SW}_\perp$ ) and for large  $\Omega$  also parallel to the polarization direction (brown,  $\text{SW}_\parallel$ ). Cyan and blue regions represent long wavelength instabilities perpendicular (cyan,  $\text{LW}_\perp$ ) and parallel (blue,  $\text{LW}_\parallel$ ) to the polarization direction.

increasing their size would lead to a loss of alignment.

To get an overview of the parameter regimes leading to different patterns we summarize the results from linear stability analysis (see [39] for further details) and simulations in a phase diagram, Fig. 4. We show in the SM [39] that the phase diagram depends only on two effective parameters:  $g\rho_0$  and  $\Omega$ . Hence, a two-dimensional visualization of the phase diagram is representative for the whole parameter space of the model (which is six/four



dimensional before/after writing the equations in their non-dimensional form). In this diagram, the red shaded domain represents parameter regimes leading to pattern formation, whereas the cyan shaded regime leads to moving bubbles. Interestingly, both regimes overlap around  $\Omega \sim 1$ , leading to coexisting short and long wavelength instabilities. This suggests that phase F is connected to a bistable set of long and short wavelength structures and that whether we find phase separation or a microflock pattern formation depends on the initial state (and on the noise realization). (We note that the instability bands associated with both instabilities are typically separated from each other by a gap (of stable wavenumbers) which prevents the pattern to coarsen even in the coexistence regime; compare also the visualizations of the dispersion relation in the SM). To test this prediction, we initialized the system in a parameter regime leading to phase separated bubbles and then change the rotating frequency to a regime where we typically observe pattern formation. Here, the phase separation remains stable as movie **3** in the SM [39] shows, confirming the existence of hysteresis.

*Conclusions* Conversely to the viewpoint that identical rotations are of no particular relevance for the collec-

tive behaviour of self-propelled particles, we show that such rotations generate a rich route to structure formation. In particular, we find that rotations which are slow compared to the rotational diffusion rate lead to the formation of rotating drops featuring an enhanced polarization as compared to the standard Vicsek model. Faster rotations generate a novel route to pattern formation yielding phase-synchronized microflocks with a characteristic size that can be tuned in practice both via the swimming speed (laser power, chemical activity) or the rotation frequency (e.g. geometry of L-shaped swimmers). Our results should be readily observable, e.g. with L-shaped phoretic colloids, and provide a general framework to understand and acknowledge the rich collective behaviour of circle swimmers. Our results can also be used to design microflock patterns of controllable size and suggest that rotations can be used as a tool to control coarsening.

*Acknowledgements* BL and DL gratefully acknowledge funding from a Marie Curie Intra European Fellowship (G.A. no 654908 and G.A. no 657517) within Horizon 2020.

BL and DL contributed equally to this work.

- 
- [1] Tailleur, J. and Cates, M. Phys. Rev. Lett. **100**, 218103 (2008).
  - [2] Cates, M. E. and Tailleur, J. Annu. Rev. Condens. Matter Phys. **6**, 219 (2015).
  - [3] Theurkauff, I., Cottin-Bizonne, C., Palacci, J., Ybert, C. and Bocquet, L. Phys. Rev. Lett. **108**, 268303 (2012).
  - [4] Palacci, J., Sacanna, S., Steinberg, A. P., Pine, D. J and Chaikin, P. M. Science **339**, 936 (2013).
  - [5] Buttinoni, I., Bialké, J., Kümmel, F., Löwen, H., Bechinger, C. and Speck, T., Phys. Rev. Lett., **110**, 238301 (2013).
  - [6] B. Liebchen, D. Marenduzzo, I. Pagonabarraga, M. E. Cates, Phys. Rev. Lett. **115** 258301 (2015).
  - [7] Levis, D., and Berthier, L. Phys. Rev. E, **89**(6), 062301, (2014).
  - [8] Vicsek, T. and Czirók, A. and Ben-Jacob, E. I and Cohen, I. and Shochet, O., Phys. Rev. Lett. **75**, 1226 (1995).
  - [9] Toner, J. and Tu, Y., Phys. Rev. Lett. **75**, 4326 (1995).
  - [10] J. B. Caussin, A. Solon, A. Peshkov, H. Chaté, T. Dauxois, J. Tailleur, V. Vitelli, and D. Bartolo Phys. Rev. Lett., **112**, 148102 (2014).
  - [11] Farrell, F. D. C, Marchetti, M. C., Marenduzzo, D. and Tailleur, J. , Phys. Rev. Lett. , **108**, 248101 (2012).
  - [12] A. P. Solon, H. Chaté, and J. Tailleur, Phys. Rev. Lett., **114**, 068101 (2015).
  - [13] Berg, H. C., and Turner, L., Biophys. J., **58**, 919 (1990).
  - [14] Di Luzio, W. R., Turner, L., Mayer, M., Garstecki, P., Weibel, D. B., Berg, H. C., and Whitesides, G. M., Nature, **435** 1271 (2005).
  - [15] E. Lauga, W. R. DiLuzio, G. M. Whitesides and H. A. Stone, Biophys. J., **90**, 400 (2006).
  - [16] R. Di Leonardo, D. Dell'Arciprete, L. Angelani and V. Iebba, Phys. Rev. Lett., **106**, 038101 (2011).
  - [17] B.M. Friedrich and F. Jülicher, Proc. Natl. Acad. Sci. **104** 13256 (2007).
  - [18] Riedel, I. H., Kruse, K., and Howard, J., Science, **309** 300 (2005).
  - [19] F. Kümmel, B. ten Hagen, R. Wittkowski, I. Buttinoni, R. Eichhorn, G. Volpe, H. Löwen and C. Bechinger, Phys. Rev. Lett, **110**, 198302 (2013).
  - [20] H. Loewen, Eur. Phys. J. **225**, 2319 (2016).
  - [21] B. Friedrich, Eur. Phys. J. **225** 2353 (2016).
  - [22] J. Denk, L. Huber, E. Reithmann, and E. Frey, Phys. Rev. Lett. **116**, 178301 (2016).
  - [23] Erglis, K., Wen, Q., Ose, V., Zeltins, A., Sharipo, A., Janmey, P. A., and Cebers, A., Biophys. J., **93**, 1402 (2007).
  - [24] Cēbers, A., Magn. Magn. Mater. **323**, 279 (2011).
  - [25] Loose, M., and Mitchison, T. J. Nat. Cell Biol., **16**, 38 (2013).
  - [26] Marchetti, M. C., Joanny, J. F., Ramaswamy, S., Liverpool, T. B, Prost, J., Rao, M., and Simha, R. A. Rev. Mod. Phys. **85**, 1143 (2013).
  - [27] Ramaswamy, S. Annu. Rev. Cond. Matt. Phys. **1**, 323 (2010).
  - [28] van Teeffelen, S. and Löwen, H., Phys. Rev. E, **78**, 020101 (2008).
  - [29] D. Dean, J. Phys. A **29**, L613 (1996).
  - [30] D. Levis, I. Pagonabarraga and A. Diaz-Guilera, arXiv preprint arXiv:1608.02423 (2016).
  - [31] E. Bertin, M. Droz, G. Gregoire, J. Phys. A, **42**, 445001 (2009).
  - [32] B. Liebchen, M. E. Cates, D. Marenduzzo, Soft Matter, **12**, 7259 (2016).
  - [33] S. Mishra, A. Baskaran, M. C. Marchetti, Phys. Rev. E, **81**, 061916 (2010).
  - [34] van Teeffelen, S., and Lowen, H. (2008). Phys. Rev. E, **78**, 020101.

- [35] Gregoire, G., and Chate, H. (2004). Phys. Rev. Lett., **92**, 025702.
- [36] Vicsek, T., and Zafeiris, A. Phys. Rep., **517**, 71-140, (2012)
- [37] Toner, J., Tu, Y., and Ramaswamy, S., Ann. of Phys., **318**, 170-244, (2005).
- [38] Gopinath, A. and Hagan, M. F. and Marchetti, M. C.. and Baskaran, A., Phys. Rev. E, **85**, 061903 (2012).
- [39] See Supplementary Material at doi:...
- [40] In Fig. 2 (j) we only show  $\lambda$  within the regime where the patterns are relatively isotropic. For higher values of  $g$ , the length scale  $\lambda$  defined from the pair correlation function gives a poor information about the shape of the microflocks and hence its formation mechanism.
- [41] Note that we find a flocking transition generally close to but slightly below the theoretical prediction, as previously noted in [11].
- [42] Note that the system typically does not reach F but forms secondary structures due to instabilities of F. However, enhanced polarization can still be observed for the (locally uniform) bubbles.